Tuning Surface Energy of Zn Anode via Sn Heteroatom Doping Enabled by a Co-Deposition for Ultralong-Lifespan Dendrite-Free Aqueous Zn-Ion Battery

Journal:	*ACS Applied Materials & Interfaces*
Manuscript ID	am-2021-06002z.R2
Manuscript Type:	Article
Date Submitted by the Author:	26-May-2021
Complete List of Authors:	Liu, Zenghua; Qingdao University of Science and Technology, College of Chemistry and Molecular Engineering Ren, Junfeng; Qingdao University of Science and Technology, School of Chemical Engineering Wang, Fanghui ; Qingdao University of Science and Technology, College of Chemical Engineering Liu, Xiaobin ; Qingdao University of Science and Technology, College of Environment and Safety Engineering Zhang, Qian; Qingdao University of Science and Technology, College of Chemistry and Molecular Engineering Liu, Jie; Qingdao University of Science and Technology, College of Chemical Engineering Kaghazchi, Payam; Forschungszentrum Jülich GmbH Ma, Dingxuan; Qingdao University of Science and Technology, College of Chemistry and Molecular Engineering Chi, Zhenzhen ; Qingdao University of Science and Technology, College of Chemistry and Molecular Engineering Wang, Lei; Qingdao University of Science and Technology, College of Environment and Safety Engineering

Tuning Surface Energy of Zn Anode via Sn Heteroatom Doping Enabled by a Co-Deposition for Ultralong-Lifespan Dendrite-Free Aqueous Zn-Ion Battery

Zenghua Liu[a,b,1], Junfeng Ren[a,c,1], Fanghui Wang[a,c], Xiaobin Liu[a,d], Qian Zhang[a,b,*], Jie Liu[a,c], Payam Kaghazchi[e], Dingxuan Ma[a,b], Zhenzhen Chi[a,b]and Lei Wang[a,d,*]

[a]*State Key Laboratory Base of Eco-chemical Engineering, Taishan Scholar Advantage and Characteristic Discipline Team of Eco-chemical Process and Technology, Qingdao University of Science and Technology, Qingdao 266042, China*

[b]*College of Chemistry and Molecular Engineering, Qingdao University of Science and Technology, Qingdao 266042, China*

[c]*College of Chemical Engineering, Qingdao University of Science and Technology, Qingdao 266042, China*

[d]*Shandong Engineering Research Center for Marine Environment Corrosion and Safety Protection, College of Environment and Safety Engineering, Qingdao University of Science and Technology, Qingdao 266042, China*

[e]*Institute of Energy and Climate Research, Forschungszentrum Jülich GmbH, Jülich 52425, Germany*

[1]*These authors contributed equally.*

ABSTRACT

Aqueous Zn-ion battery has been considered as one of the most promising large-scale energy storage systems, owing to the advantages of raw materials abundance, low cost, and eco-friendliness. However, the severe growth of Zn dendrites leads to poor stability and low coulombic efficiency of aqueous Zn-ion battery. Herein, to effectively inhibit the growth of Zn dendrites, a new strategy has been proposed, i.e., tuning the surface energy of Zn anode. This strategy can be achieved by in-situ doping of Sn heteroatom in the lattice of metallic Zn via co-deposition of Sn and Zn with a small amount of $SnCl_2$ electrolyte additive. DFT calculations have suggested that Sn heteroatom doping can sharply decrease the surface free energy of Zn anode. As a consequence, driven by the locally strong electric field, metallic Sn tends to deposit at the tips on Zn anode, thus decreases the surface energy and growth of Zn at the tips, resulting in a dendrite-free Zn anode. The positive effect of $SnCl_2$ additive has been demonstrated in both Zn‖Zn symmetric battery and Zn/LFP, Zn/HATN full cell. This novel strategy can light a new way to suppress Zn dendrites for long-lifespan Zn-ion batteries.

KEYWORDS: aqueous Zn-ion battery, dendrite-free Zn anode, surface energy, electrolyte additive, ultralong lifespan

INTRODUCTION

Rechargeable metal-ion batteries have been developed rapidly due to the ever-increasing demand in electric vehicles and portable electronics. Li-ion battery, with high energy density and long lifespan, has dominated the market of energy storage for several years.[1,2] Nevertheless, the drawbacks including the high price and uneven distribution of lithium resources as well as the flammability and toxicity of organic electrolytes have severely hampered the broad applications of Li-ion batteries.[3,4] Recently, aqueous Zn-ion battery has attracted intensive attentions, owing to the advantages of low cost, environmental friendliness, raw material abundance, and high theoretical capacity (820 mAh g^{-1}).[5-9]

Different from traditional alkaline Zn metal battery, aqueous Zn-ion battery (AZB) uses weak acid solution as electrolyte and presents much better reversibility and higher capacity retention.[10] Several Zn^{2+} salts have been reported as the electrolyte of AZB. Among them, $ZnCl_2$, $Zn(NO_3)_2$, and $Zn(ClO_4)_2$ are considered to be not suitable as the electrolyte for high-performance AZBs because of their intrinsic deficiencies such as narrow anodic potential window ($ZnCl_2$), strong oxidizing ($Zn(NO_3)_2$ and $Zn(ClO_4)_2$), as well as relatively high overpotential ($Zn(ClO_4)_2$).[11-13] In contrast, $Zn(CF_3SO_3)_2$ and $Zn(TFSI)_2$ aqueous electrolyte solutions exhibit remarkable electrochemical performances by facilitating the kinetic of Zn^{2+} transfer and enhancing the stability of Zn anode.[14,15] However, the high expense of these electrolytes will limit their large-scale application in commercial AZBs. $ZnSO_4$ electrolyte solution, with the advantages of low cost, good stability, and acceptable performances for most cathodes,[16-19] holds great application potential and has been widely used in AZBs.

Despite the exciting superiorities and promising prospect of AZBs based on $ZnSO_4$ electrolyte solution, the severe dendrite issue caused by the uneven deposition of metallic Zn, which leads to poor reversibility and low coulombic efficiency of Zn-ion battery, is urgently demanded to be addressed.[20,21] The nucleation and growth

of Zn dendrite are driven by locally strong electrical field, partially high concentration of Zn^{2+} ions, and high surface energy of protuberances on Zn anode.[22] Therefore, the growth of Zn dendrite is able to be inhibited by regulating the electrical field on Zn anode, the Zn^{2+} ion transmission between electrolyte and the electrode, and the surface energy of Zn anode. The 3D structure can lead to a uniform distribution of the electric field on Zn anode, resulting in homogeneous deposition of Zn particles and improving the stability of aqueous Zn-ion battery. Therefore, Zn anodes with 3D structural substrate like CNT,[23] MXene,[24] MOF,[25] and foam Cu etc.[26] have been designed. In the case of controlling Zn^{2+} ion concentration on Zn anode, several strategies have also been proposed: (i) Accelerating the transmission of Zn^{2+} ion by covering a coating layer with high ionic conductivity and good affinity with electrolytes on the surface of Zn electrode, such as ultrathin TiO_2 film,[27] nano-ZrO coating,[28] MXene,[29] kaolin coating[30] and ZIF-8 coating,[31] which promotes the extensive nucleation of metallic Zn on Zn anode; (ii) Uniformizing Zn^{2+} ion transference on the surface of Zn electrode through adding organic additives such as polyacrylamide (PAM),[32] diethyl ether (Et_2O),[33] tetrabutylammonium sulfate (TBA^+),[34] neutral ligand (succinonitrile, SN)[35] (Referee 1) and sodium dodecyl benzene sulfonate (SDBS)[36] in the electrolyte solution. The highly-polar molecules preferentially adsorbed on the tip sites of Zn electrode as a shield layer and guided Zn deposition on the flat region of Zn electrode.

Nevertheless, to our best knowledge, the strategy to restrain Zn dendrite by regulating the surface energy of Zn anode is rarely reported. It is evidenced that doping heteroatom in the lattice of host benefits to decrease the surface free energy of the host.[37,38] Co-deposition is a practical way to achieve the in-situ doping of heteroatom in the lattice of metallic Zn.[39] Hence, we proposed a new strategy of inhibiting the growth of Zn dendrite by decreasing the surface energy of Zn anode through adding a small amount of economic $SnCl_2$ additive in $ZnSO_4$ electrolyte solution. Although the Zn|Sn anode has been reported in several recent advances of AZBs, where coating, CVD and hot dipping methods are applied to construct Zn|Sn alloy[40-42], the synthetic process and materials needed to achieve these strategies are usually complex and

expensive, which is not facile for a large-scale application. However, our strategy aims at the electrolyte modification of AZB with a very simple method, that is, adding a small amount of $SnCl_2$ and $C_6H_5Na_3O_7·2H_2O$ additive in $ZnSO_4$ solution without any further treatment. This strategy is very easily to be scaled-up for a large-scale application. Moreover, with this very simply strategy we can also successfully inhibit the Zn dendrite formation, corrosion and hydrogen evolution during the charging/discharging process. According to the DFT calculation results, doping Sn atom in the lattice of Zn can remarkably decrease the surface free energy of low-index Zn surfaces. Experimentally, with $SnCl_2$ additive, the overpotiential of Zn platting/stripping has been sharply reduced and the lifespan of Zn‖Zn symmetric cell has extremely extended to 2000 h. Especially, the Zn/HATN full cell with $SnCl_2$ additive performs excellent stability with an ultra-long cycling life of ~10000 cycles, suggesting the application potential of the $SnCl_2$ electrolyte additive.

MATERIAL and METHOD

Preparation of Electrolyte

$ZnSO_4·7H_2O$ (Macklin, 99.95%), $C_6H_5Na_3O_7·2H_2O$ (Guoyaoreagent, AR) and $SnCl_2·2H_2O$ (AR) were utilized directly to prepare the electrolyte of aqueous Zn-ion battery without further treatment, 0.078 g $SnCl_2·2H_2O$ and 1.029 g $C_6H_5Na_3O_7·2H_2O$ (the molar ratio of $SnCl_2·2H_2O$ and $C_6H_5Na_3O_7·2H_2O$ is 1:10) were added into 5 mL 2.0 M $ZnSO_4$ solution and stirred thoroughly until the materials completely dissolved to add 7.0 mM$SnCl_2$ in 2.0 M $ZnSO_4$ solution. $C_6H_5Na_3O_7·2H_2O$ was added as complex agent to prevent the hydrolysis of $SnCl_2$. $ZnSO_4$ electrolyte with different concentrations of $SnCl_2$ (3.0 mM, 5.0 mM and 10.0 mM) were also prepared with similar process. Simultaneously, 2.0 M $ZnSO_4$ without $SnCl_2$ additive was also prepared for comparison.

Material Characterization

Scanning electron microscope (SEM) images were observed on a regulus8100 field emission scanning electron microscope, and elemental mapping was obtained on an EDAX Genesis energy dispersive X-ray fluorescence spectrometer. X-ray powder

diffraction (XRD) measurements were carried out via a Bruker D8 Advance powder X-ray diffractometer with a scan speed of 5° min^{-1} in the range of 10°-80°. X-ray photoelectron spectroscopy (XPS) spectra were obtained on a Thermo ESCALAB 250XI (Mg K Alpha) photoelectron spectrometer. Inductive coupled high frequency plasma optical emission spectrometer (ICP-OES) was tested on Agilent 730.

Electrochemical Measurements

Zn‖Zn and battery was assembled with 2016-type coin cells using Zn foils as cathode and anode, glass fiber as separator, and 2.0 M $ZnSO_4$ without/with $SnCl_2/C_6H_5Na_3O_7$ as electrolyte.

The $LiFePO_4$ powder (LFP) (KJ GROUP P198-S21), Super P (Sinopharm Chemical Reagent Co., Ltd) and polyvinylidene fluoride (PVDF) (Sinopharm Chemical Reagent Co., Ltd.) with a mass ratio of 8 : 1 : 1 were mixed in N-methyl-2-pyrrolidinone (NMP) (Alfa Aesar, ≥99%) to prepare the cathode of Zn/LFP battery. The slurry was uniformly coated on titanium foil and dried at 60 °C overnight in a vacuum oven. The mass loading of LFP was about 2.0 mg cm^{-2}. The 2032-type coin cells were assembled using as-prepared LFP cathode, Zn foil, glass fiber, and 1.0 M $ZnSO_4$ + 1.0 M Li_2SO_4 without/with $SnCl_2/C_6H_5Na_3O_7$ as cathode, anode, separator, and electrolyte, respectively.

The diquinoxalino [2, 3-a:2',3'-c] phenazine (HATN) powder, Super P and PVDF with a mass ratio of 6.5 : 3 : 0.5 were mixed in NMP to prepare the cathode of Zn/HATN battery. The slurry was uniformly coated on titanium foil and dried at 60 °C overnight in a vacuum oven. The mass loading of HATN was about 0.7 mg cm^{-2}. The 2032-type coin cells were assembled using as-prepared HATN cathode, Zn foil, glass fiber, and 2.0 M $ZnSO_4$ with $SnCl_2/C_6H_5Na_3O_7$ as cathode, anode, separator, and electrolyte, respectively.

Galvanostatic charge/discharge cycling tests were carried out by using a battery test system (LAND CT2001A) in voltage range of 0.8-1.5 V (LFP) and 0.3-1.1 V (HATN). Cyclic voltammetry (CV) measurements were performed using a VSP electrochemical workstation. The scan rates are set to be 0.1 mV s^{-1} for Zn/LFP full cell and 5 mV s^{-1} for Zn/HATN full cell, respectively. Electrochemical impedance

spectroscopy (EIS) test was carried out in Princeton at a frequency range of 10^{-2}-10^{5} Hz with an amplitude of 5.0 mV.

Hydrogen Evolution Experiment

Hydrogen evolution experiment was performed with an in-situ Raman cell assembled using Cu foil, Zn foil, and 2.0M ZnSO4 solution with/without 7.0 mM $SnCl_2$ as working electrode, counter electrode, and electrolyte respectively. The hydrogen evolution was observed under an optical microscope and recorded with a digital camera for 20 min at a current density of 10mA cm^{-2}.

Theoretical Method

Density functional theory (DFT) calculations were carried out using the Projector-Augmented Wave (PAW) method as implemented in the Vienna Ab Initio Simulation Package (VASP). [43] For the exchange-correlation functional, we used the Perdew-Burke-Ernzerhof (PBE)[44] of Generalized-Gradient Approximation with the Hubbard *U* parameter proposed by Dudarev.[45] In our calculations, the value of U_{eff} for Zn was set to be 5.0 eV. The (001), (101), (100), and (110) surface of Zn and Sn-doped Zn were modeled with 64 atoms. 16 atoms (one layer for (001), (101) surface and 2 layers for (100), (110) surface) on the bottom were fixed. A vacuum size of 12 Å was applied to prevent the interaction between periodic images along the *c* direction. A *k*-point mesh of 2×2×1 was used for surface calculations. An energy cutoff of 300 eV as well as a force convergence criterion of 0.001 eV $Å^{-1}$ were applied for both bulk and surface calculations. The surface free energy was calculated by equation:

$$\gamma = 1/A\ (E_{surf} - E_{bulk}),$$

where E_{surf}, E_{bulk} are the total energy of the surface and bulk, respectively. A is the surface area.

RESULTS WITH DISCUSSION

To decrease the surface free energy of Zn anode, a co-deposition of metallic Sn and Zn via introducing a small amount of $SnCl_2$ additive in $ZnSO_4$ electrolyte solution

has been designed to realize the in-situ doping of Sn heteroatom in the lattice of metallic Zn. Density functional theory (DFT) calculations were firstly processed to calculate and compare the surface free energy (γ) of Zn surfaces without and with Sn doping. Four low-index planes (001), (101), (100), and (110) were considered. To simulate Zn surfaces with Sn dopant, one Zn atom in the top layer of the surfaces was replaced by one Sn atom (**Figure 1a**). The atom ratio of Zn and Sn in the model of Zn surfaces was kept to be 63 : 1. The calculated surface free energies indicate that (001) surface is more favorable than (101), (100) and (110) surface for both bare and Sn-doped Zn (i.e., $\gamma_{(001)} < \gamma_{(101)} < \gamma_{(100)} < \gamma_{(110)}$). As shown in **Figure 1b,** the calculated surface free energy of (001), (101), (100) and (110) surface for bare Zn are 0.067, 0.102, 0.118 and 0.162 eV $Å^{-2}$, respectively. Interestingly, the values are sharply decreased to 0.049, 0.058, 0.081 and 0.104 eV $Å^{-2}$ respectively after replacing one Zn atom by Sn atom. As a consequence, during the platting process of AZB, driven by the partially strong electric field, metallic Sn tends to deposit at the protuberances on Zn anode, thus decreases the surface free energy and growth of Zn at the tips, resulting in a dendrite-free Zn anode.

Inspired by the DFT calculations, economical $SnCl_2$ was applied as the additive for $ZnSO_4$ electrolyte solution in AZB to achieve the in-situ Sn doping in the lattice of metallic Zn. Firstly, influence of $SnCl_2$ concentration on the performance of AZB was studied. A series of $ZnSO_4$ electrolyte solutions were prepared through adding different concentrations of $SnCl_2$ (0.0, 3.0, 5.0, 7.0, and 10.0 mM) into 2.0 M $ZnSO_4$ solution. In order to prevent the hydrolysis of $SnCl_2$, sodium citrate ($C_6H_5Na_3O_7$, molar ratio of 10:1 to $SnCl_2$) as stabilizer was also added into the $ZnSO_4$ solution. As shown in **Figure S1**, all $ZnSO_4$ solutions with $SnCl_2$ additive were dissolved completely after fully stirring. However, only $ZnSO_4$ solutions with 7.0 mM and 10.0 mM $SnCl_2$ additive remain transparent after 72 h standing, indicating a better stability of the solutions. Subsequently, Zn‖Zn symmetric battery was assembled using $ZnSO_4$ electrolyte solution with $SnCl_2$ in different concentrations. **Figure 2a** shows the polarization curves of Zn‖Zn symmetric battery at a constant current density of 0.5 mA cm^{-2}. It indicates that all $ZnSO_4$ electrolyte solutions with $SnCl_2$ additive show

much decreased overpotential compared to the bare $ZnSO_4$ electrolyte solution, and $ZnSO_4$ electrolyte with 7.0 mM $SnCl_2$ additive (in red color) depicts superior Zn stripping/plating behavior compared to $ZnSO_4$ electrolyte with $SnCl_2$ under other concentrations (0.0, 3.0, 5.0, and 10.0 mM).

The voltage profiles of Zn‖Zn symmetric battery at 1st, 2nd, 417th, 418th and 500th cycle were enlarged and presented in **Figure 2b-d**. The overpotential of Zn‖Zn symmetric cell with 7.0 mM $SnCl_2$ additive starts at 50.6 mV and drops quickly to 19.9 mV at 2nd cycle. It is kept below 20.0 mV until 417 h, then slightly increases to ~24.0 mV and stabilizes until 600 h with no sign of cell short-circuiting. In stark contrast, the overpotential of Zn‖Zn symmetric cell without $SnCl_2$ additive is around 117.0 mV at beginning, which fluctuates between 44.2 and 68.2 mV in following cycles until 494 h. After 494 h, the value starts to increase exponentially, which indicates the failure of the battery. The lower overpotential of Zn‖Zn symmetric cell demonstrates a more stable and faster kinetics of Zn stripping/plating process in the $ZnSO_4$ electrolyte with $SnCl_2$ additive. To highlight the effect of $SnCl_2$ additive, voltage profiles of Zn‖Zn symmetric cell with 2.0 M $ZnSO_4$ and 70.0 mM $C_6H_5Na_3O_7$ electrolyte solution are presented in **Figure S2**. It is suggested that $C_6H_5Na_3O_7$ possesses adverse effect on the electrochemical performance of AZB. The poor cycling stability of Zn‖Zn symmetric cells with 3.0 and 5.0 mM $SnCl_2$ additive is due to the poor stability of the electrolyte solutions, while for Zn‖Zn symmetric cell with 10.0 mM $SnCl_2$ additive, it may result from the high content of $C_6H_5Na_3O_7$. A long lifespan polarization curve of Zn‖Zn symmetric cell with 7.0 mM $SnCl_2$ at a current density of 0.5 mA cm^{-2} is also depicted in **Figure 2e**. The voltage profile shows remarkable stability for 2000 h with no sign of battery death, which is superior to most of the electrolytes or additives previously reported (**Table S1**).[12,13,15,16,32-34,36,46-48] **Figure 2f** displays the rate performance of Zn‖Zn symmetric cell with $SnCl_2$ at a series of current densities of 0.5, 1.0, 2.0, 3.0, 5.0, and 0.5 mA cm^{-2}, respectively. It is shown that the overpotential is only 52.2 mV at high current density of 5.0 mA cm^{-2} and decreases back to 10.0 mV when the current density decreases to 0.5 mA cm^{-2} again, suggesting the excellent rate behavior. The galvanostatic cycling curves at high current density of 2.0 mA cm^{-2} of

Zn‖Zn symmetric battery without/with $SnCl_2$ additive are shown in **Figure 2g**. The symmetric cell with $SnCl_2$ additive can still exhibit an outstanding cycling stability for 300 h with a low overpotential of 40.0 mV, which is greatly superior to the cell without additive. To further explore the effect of $SnCl_2$ additive on Zn‖Zn symmetric battery with large depth of discharge and high areal capacity, cycling performances at 3 mA cm^{-2} and 3 mAh cm^{-2} are shown in **Figure S3**. It is observed from **Figure S3** that although the overpotential of Zn‖Zn symmetric battery using electrolyte with $SnCl_2$ additive is not obviously decreased compared to the values without $SnCl_2$ additive, cycling stability of the symmetric battery is greatly improved when $SnCl_2$ additive is added into the electrolyte. The Zn‖Zn symmetric battery without additive failed after only 45 h because of the dendrite formation. However, Zn‖Zn symmetric battery with $SnCl_2$ additive can cycle stably for 140 h without any signal of failure. The enhanced electrochemical performance of Zn‖Zn symmetric battery with $SnCl_2$ additive results from the dendrite-free Zn anode with stable and facile Zn platting/stripping achieved by Sn doping.

To illustrate the change of Zn electrode during Zn deposition process, ex-situ optical microcopy images are observed and shown in **Figure 3a**. The surface of Zn electrode got completely black after 40 min in the $ZnSO_4$ electrolyte without additive, which indicates the generation of "dead Zn" during deposition process.[49,50] However, Zn electrode in the $ZnSO_4$ electrolyte with $SnCl_2$ additive keeps bright until 40 min with only sporadic protuberances. To further observe the morphology of Zn electrode after cycling of Zn‖Zn symmetric cell, SEM images are also tested and presented in **Figure 3b-f**. The morphology of commercial Zn foil before cycling is smooth and flat (**Figure 3b**). However, after 500 cycles, hexahedral sheets were accumulated perpendicular to the surface of Zn anode in $ZnSO_4$ electrolyte without additive, demonstrating the generation and growth of Zn dendrite (**Figure 3c,d**).[51,52] On the contrary, when $SnCl_2$ was added into $ZnSO_4$ electrolyte solution, a smooth morphology with nanopores is observed after 500 Zn plating/stripping cycles (**Figure 3e,f**). Furthermore, the SEM image with larger magnification in **Figure 3f** shows that

the growth of Zn dendrites on Zn electrode is effectively suppressed owing to the addition of $SnCl_2$. It is speculated from the SEM images that metallic Sn has deposited simultaneously with Zn during the Zn electro-deposition process. As indicated by the DFT calculations, the deposition of Sn at the tips on Zn electrode decreases the surface energy of Zn electrode. Then the growth of Zn crystal at the tips is therefore refined, which reflects to a smooth morphology after cycling. The nanopores on Zn anode are considered to be caused by the stack of refined Zn particles. XRD patterns of Zn anode after 100 cycles in $ZnSO_4$ electrolyte without and with $SnCl_2$ additive are illustrated in **Figure 3g and Figure S4**. The peaks of Zn anode without additive located at 36.34°, 39.06°, 43.28°, 54.38°, 70.14°, and 70.66° are indexed to the (002), (100), (101), (102), (103), and (110) planes of Zn (JCPDS card:04-0831), respectively. Additionally, three extra peaks located at 28.48°, 31.56°, and 34.27° are corresponding to ZnO (28.48°) and $Zn_4(OH)_6SO_4$ $4H_2O$ (31.56°, and 34.27°) [53,54] respectively. Therefore severe side reactions occur on Zn anode in electrolyte without additive. When $SnCl_2$ is added into $ZnSO_4$ electrolyte, the location of peaks for (002), (100), (101), (102), and (110) planes are slightly shifted to 36.39°, 39.08°, 43.31°, 54.40°, and 70.70°, respectively. DFT calculations show that the interlayer distance d_{hkl} of (001), (100), (101), and (110) planes are decreased after the doping of Sn atom in the lattice of Zn (**Figure S5**). According to the Bragg's Law: $2d_{hkl}\sin\theta = c\lambda$,[55] the diffraction angle 2θ is increased as the value of d_{hkl} decreases. Therefore, it is evidenced through the shift of peaks in XRD pattern that Sn atom has successfully doped in the Zn lattice via the addition of $SnCl_2$ additive in $ZnSO_4$ electrolyte. Moreover, no extra peaks have been tested on Zn anode in electrolyte with $SnCl_2$ additive, demonstrating that $SnCl_2$ additive can greatly suppress the side reactions on Zn anode. EDS-Mapping analysis has been conducted for Cu electrode of Zn/Cu asymmetric battery after 10 cycles in electrolyte containing $SnCl_2$ **(Figure 3h and Figure S6)**. It is evidenced by EDS and Mapping analysis that, metallic Sn has been successfully and uniformly deposited on the surface of Cu electrode. According to the EDS analysis (**Figure S6a)**, the deposition ratio of Sn on Zn surface is 2.31% (0.53/(22.20+0.53)·100). Moreover, ICP measurement (**Figure**

S6b) also shows that the deposition ratio of Sn on Zn surface is ~2.9%. Furthermore, ex-situ XPS analysis was conducted for Zn anode in Zn‖Zn symmetric cell without and with $SnCl_2$ additive after 500 cycles (**Figure 3i, j** and **Figure S7**). The existence of Sn 3d peak (**Figure 3i**) and the peak position at 1023.28 eV of Zn 2p (**Figure 3j**), which corresponds to the Zn-O-Sn compound (oxidized Zn with doped Sn),[56,57] highlight again that metallic Sn has successfully deposited on the surface of Zn anode during the plating/stripping process.

To explore the deposition mechanism of metallic Zn in electrolyte without/with $SnCl_2$ additive during Zn plating process, electrochemical impedance spectroscopy (EIS) was performed using three-electrode system at frequency ranging from 10^5 Hz to 10^{-2} Hz with an amplitude of 5 mV. As shown in **Figure 4a** and **Figure S8**, when the pristine Zn plate was inserted into 2.0 M $ZnSO_4$ electrolyte without additive, the equivalent circuit can be described as $LR_s(Q_1R_f)(Q_2R_{ct})$. In this model, Rs represents the solution resistance, R_f is caused by a thin layer of ZnO on the Zn anode, and R_{ct} is the electric transfer resistance. After 10 cycles, the equivalent circuit of the impedance spectra changes to $LR_S(Q_1(R_f(Q_2R_{ct}))$. A porous surface (Q_1), which can be caused by the irregular stack of Zn dendrites, has generated during the Zn platting/stripping process.[58] This porous structure has also been observed in the SEM images of **Figure 3d**. As shown in **Figure 4b** and **Figure S9**, when Zn plate was immersed into $ZnSO_4$ electrolyte with $SnCl_2$ additive, the equivalent circuit turns to $LR_s(Q_0R_1)(Q_1(R_f(Q_2R_{ct})))$. A complex film caused by the equilibrium absorption of Zn^{2+}, Sn^{2+} and citrate on the surface of ZnO layer has formed. After 10 cycles, as illustrated by the equivalent circuit $LR_s(Q_1R_f)(Q_2(R_{ct}W)$, a Zn/Sn coating layer has been constructed on the surface of Zn electrode. The existence of Zn/Sn coating layer prevents the excessive growth of Zn crystal and leads to a smoother morphology on Zn electrode after cycling. Furthermore, the low frequency impedance values listed in **Table S2** demonstrate that impedance of three-electrode system in 2.0 M $ZnSO_4$ electrolyte with $SnCl_2$ additive has dramatically decreased after cycling. This decrease is probably caused by the degradation of ZnO and the smoothly deposited Zn/Sn layer on Zn anode during cycling. In sharply contrast, the impedance of three-electrode

system in bare $ZnSO_4$ electrolyte has slightly increased, which is led by the formation of Zn dendrites.

Depending on the SEM images, XPS analysis and the EIS results, a schematic diagram of Zn/Sn co-deposition mechanisms in $ZnSO_4$ solution without/with $SnCl_2$ additive was presented in **Figure 4c and Figure 4d**. In short, metallic Zn and Sn co-deposited/dissolved reversibly on/from Zn anode during charging/discharging process. The metallic Sn is prior to deposit on the protuberance sites driven by the partially strong electric field. The deposition of Sn benefits to decrease the surface energy of Zn anode with smaller Zn dendrite size, which leads to a uniform and smooth Zn morphology on Zn anode and therefore remarkably improves the cycle performance of Zn‖Zn symmetric cell. The electrochemical behavior of Zn foil in 2.0 M $ZnSO_4$ solution without/with additive was also tested with Tafel curves using three-electrode system. **Figure S10** illustrates the Tafel curves of Zn plate in 2.0 M $ZnSO_4$ without/with $SnCl_2$ additive. As shown in **Figure S10,** the corrosion current of Zn plate in $ZnSO_4$ electrolyte with $SnCl_2$ additive (2.36 mA cm^{-2}) is smaller than the corrosion current of Zn plate in $ZnSO_4$ electrolyte without additive (2.96 mA cm^{-2}). Therefore, the corrosion reaction has been successfully resisted when $SnCl_2$ is added into $ZnSO_4$ electrolyte [59] Combined with the SEM images in **Figure 3**, it is concluded that the lower corrosion reaction occurred on the surface of Zn plate can effectively suppress the growth of Zn dendrites. Hydrogen evolution experiments were also performed to explore the effect of $SnCl_2$ additive on inhibiting hydrogen evolution during electrochemical process. As illustrated in **Figure S11**, vast large bubbles formed on the surface of Zn foil and Cu foil, indicating severe hydrogen evolution during Zn electroplating/stripping process in $ZnSO_4$ electrolyte without $SnCl_2$ additive; In contrast, only sporadic small bubbles have been observed on Cu foil surface in $ZnSO_4$ electrolyte with $SnCl_2$ additive. Therefore, hydrogen evolution has been effectively suppressed owing to the addition of $SnCl_2$ in $ZnSO_4$ electrolyte.

To evaluate the application potential of this novel electrolyte additive, Zn/LFP full cells were assembled using commercial $LiFePO_4$ (LFP) as cathode, Zn foil as anode, glass fiber as separator, and 1.0 M $ZnSO_4$+1.0 M Li_2SO_4 solution without/with $SnCl_2$

additive as electrolyte. The SEM images of this commercial LFP are shown in **Figure S12**, indicating the micro-size of LFP particles. **Figure 5a** presents the cycle performance of Zn/LFP full cell at current density of 5 C (1 C = 170 mAh g^{-1}). The discharge capacity of Zn/LFP full cell without additive at 1st and 50th cycle are 76.3 and 50.5 mAh g^{-1}, respectively, which corresponds to a capacity retention ratio of 66.19%. However, when $SnCl_2$ additive was added to the electrolyte, the discharge capacity of 1st and 50th cycle are 74.9 and 60.9 mAh g^{-1}, respectively, with a higher capacity retention ratio of 81.31% after 50 cycles. Additionally, **Table S3** also listed the initial coulombic efficiency of Zn/LFP full cell without/with $SnCl_2$ additive. It can be seen that the initial coulombic efficiency of Zn/LFP full cell with $SnCl_2$ additive is higher than the Zn/LFP full cell without additive, suggesting that $SnCl_2$ additive can improve the reversibility of Zn/LFP full cell. The CV curves of the 1st cycle for Zn/LFP full cell without/with additive are shown in **Figure 5b**. An obvious right shift is observed on the reduction peak when $SnCl_2$ was added to $ZnSO_4$ electrolyte, which indicates a smaller polarization of Zn/LFP full cell with additive. Rate performances of Zn/LFP full cell without and with $SnCl_2$ additive have also been tested and illustrated in **Figure 5c.** As shown in Figure 5c, the capacity of Zn/LFP full cell with $SnCl_2$ additive at current rate of 2, 3, 4, 5 C are 120.6, 97.1, 81.2, 68.4 mAh g^{-1}, respectively, which are higher than Zn/LFP full cell without $SnCl_2$ additive (124.9, 93.0, 73.9, 56.3). Therefore, the rate performance of Zn/LFP full cell was also improved after the addition of $SnCl_2$ additive. **Figure 5d-g** present the SEM images of Zn anode in Zn/LFP full cell after 50 cycles. A rough morphology formed caused by the growth of Zn dendrites on Zn anode when bare $ZnSO_4$ solution was utilized as electrolyte. In contrast, a smooth and homogeneous morphology was observed when $SnCl_2$ additive was added into the electrolyte, proving an effective inhibition of $SnCl_2$ additive to the growth of Zn dendrites. Although manganese-based, vanadium-based and prussian blue cathode materials all have promising application potential in AZBs, the toxic heavy metals in the cathode materials have harmful impacts on human body and environment. Therefore, organic materials have been explored to be cathode of AZBs due to the character of environmentally friendliness. [60-62] Herein, organic

diquinoxalino [2,3-a:2',3'-c] phenazine (HATN) material (**Figure S13**) was also prepared with the method reported previously.[8] The cycling performance of Zn/HATN full cell using 2.0 M $ZnSO_4$ electrolyte without and with $SnCl_2$ additive was tested and presented in **Figure 5h**. A small current density (0.1 A g^{-1}) was conducted on the full cell at the first three cycles for battery activation. Although ultra-long cycling life of 9999 cycles have been achieved in both Zn/HATN full cell without and with additive, the cycling stability and capacity retention ratio are obviously improved when $SnCl_2$ additive was added to the electrolyte. Impressively, the retained discharge capacity of Zn/HATN full cell with $SnCl_2$ additive after 9999 cycles is 118.1 mAh g^{-1}, which is much higher than the full cell without additive (58.3 mAh g^{-1}). Moreover**,** the initial coulombic efficiency (**Table S3)** of Zn/HATN full cell with $SnCl_2$ additive is as high as 96.58%, indicating the excellent reversibility of Zn/HATN full cell with additive. CV curves displayed in **Figure 5i** shows that an obvious right shift is observed on the reduction peak when $SnCl_2$ was added to $ZnSO_4$ electrolyte, indicating smaller polarization of Zn/HATN full cell with $SnCl_2$additive. Finally, rate performances of Zn/HATN full cell without and with $SnCl_2$ additive were also compared and exhibited in **Figure 5j**. The discharge capacity of Zn/HATN full cell with $SnCl_2$ additive at current density of 1, 2, 3, 4, 5 A g^{-1} are 155.3, 133.5, 120.7, 112.3, and 107.7 mAh g^{-1}, respectively, which are much higher than Zn/HATN full cell without additive (117.6, 79.2, 52.5, 42.9, and 37.5 mAh g^{-1}). Moreover, Zn/HATN full cell with additive can still maintain an average discharge capacity of 140.5 mAh g^{-1} when the current density comes back to 1 A g^{-1}. Therefore, $SnCl_2$ additive can greatly improve the rate performance of Zn/HATN full cell.

CONCLUSIONS

The severe growth of Zn dendrites during cycling of AZB has been effectively inhibited via a new strategy, i.e., achieving the in-situ doping of heteroatom Sn in the lattice of metallic Zn through the addition of a slight amount of $SnCl_2$ electrolyte additive. The co-deposition of metallic Sn with Zn has dramatically decreased the surface energy of Zn anode, therefore refined the Zn particles grown on Zn electrode

and suppressed the growth of Zn dendrites during the charging/discharging process. As a result, the Zn‖Zn symmetric battery using $ZnSO_4$ electrolyte with $SnCl_2$ additive performs outstanding stability over 2000 h with sharply decreased overpotential. A much higher capacity retention ratio (81.31%) is obtained after 50 cycles in the Zn/LFP full cell with $SnCl_2$ additive compared to that without additive (66.19%). Impressively, the Zn/HATN full cell with $SnCl_2$ additive exhibits remarkable cycling stability with an ultra-long cycling life of ~10000 cycles. These superior electrochemical performances have powerfully demonstrated the application potential of the novel $SnCl_2$ electrolyte additive.

ASSOCIATED CONTENT

Supporting Information

Additional details and figures as described in the text.

Conflict of Interests

The authors declare no competing financial interest.

AUTHOR INFORMATION

Corresponding Author

*Email: q_Zhang2020@126.com (Q. Zhang)

*Email: inorchemwl@126.com (L. Wang)

AUTHOR CONTRIBUTIONS

Z.L. and J.R contributed equally. All authors participated data analysis, result discussion and contributed to paper writing and revision.

ACKNOWLEDGMENT

This study was financially supported by the Taishan Scholars Project of Shandong Province, the National Natural Science Foundation of China (51802171, and 22005169), the Applied Research Project for Postdoctoral Researcher of Qingdao

City, the Natural Science Foundation of Shandong Province (ZR2020QB121), Outstanding Youth Foundation of Shandong Province (ZR2019JQ14).

REFERENCES

1. Liu, J.; Galpaya, D. G. D.; Yan, L.; Su, M. M.; Zhang, S. Exploiting a Robust Biopolymer Network Binder for an Ultrahigh-Areal-Capacity Li–S Battery. *Energy Environ. Sci.* **2017**, 10, 750-755.
2. Luo, J.; Cui, W.; He, P.; Xia, Y. Raising the Cycling Stability of Aqueous Lithium-Ion Batteries by Eliminating Oxygen in the Electrolyte. *Nat. Chem.* **2010**, 2, 760-765.
3. Yang, Y.; Tang, Y.; Fang, G.; Shan, L.; Guo, J.; Zhang, W.; Wang, C.; Wang, L.; Zhou, J.; Liang, S. Li^+ Intercalated $V_2O_5{\cdot}nH_2O$ with Enlarged Layer Spacing and Fast Ion Diffusion as an Aqueous Zinc-Ion Battery Cathode. *Energy Environ. Sci.* **2018**, 11, 3157-3162.
4. Wang, D.; Li, H.; Liu, Z.; Tang, Z.; Liang, G.; Mo, F.; Yang, Q.; Ma, L.; Zhi, C. A Nanofibrillated Cellulose/Polyacrylamide Clectrolyte-Based Flexible and Sewable High-Performance Zn-MnO_2 Battery with Superior Shear Resistance. *Small* **2018**, 14, 1803978.
5. Kundu, D.; Adams, B. D.; Duffort, V.; Vajargah, S. H.; Nazar, L. F. A High-Capacity and Long-Life Aqueous Rechargeable Zinc Battery Using a Metal Oxide Intercalation Cathode. *Nat. Energy* **2016**, 1, 1-8.
6. Pan, H.; Shao, Y.; Yan, P.; Cheng, Y.; Han, K. S.; Nie, Z.; Wang, C.; Yang, J.; Li, X.; Bhattacharya, P. Reversible Aqueous Zinc/Manganese Oxide Energy Storage From Conversion Reactions. *Nat. Energy* **2016**, *1,* 39.
7. Parker, K. F.; Chervin, C. N.; Pala, I. R.; Machler, M.; Burz, M. F.; Long, J. W.; Rolison, D. R. Rechargeable Nickel–3D Zinc Batteries: An Energy-Dense, Safer Alternative to Lithium-Ion. *Science* **2017**, 356*,* 415-418.
8. Tie, Z.; Liu, L.; Deng, S.; Zhao, D.; Niu, Z. Proton Insertion Chemistry of Zn/Organic Battery. *Angew. Chem., Int. Ed.* **2020**, 132 (12).
9. Ming, J.; Guo, J.; Xia, C.; Wang, W.; Alshareef, H. N. Zinc-Ion Batteries: Materials, Mechanisms, and Applications. *Mater. Sci. Eng. R.* **2019**, 135, 58-84.
10. Zhang, T.; Tang, Y.; Guo, S.; Cao, X.; Pan, A.; Fang, G.; Zhou, J.; Liang, S. Fundamentals and Perspectives in Developing Zinc-Ion Battery Electrolytes: a Comprehensive Review. *Energy Environ. Sci.* **2020**, 13, 4625-4665.
11. Zhang, C.; Holoubek, J.; Wu, X.; Daniyar, A.; Zhu, L.; Chen, C.; Leonard, D. P.; Rodríguez-Pérez, I. A.; Jiang, J. X.; Fang, C. A $ZnCl_2$ Water-in-Salt Electrolyte for a Reversible Zn Metal Anode Electronic Supplementary Information (ESI) Available. *Chem. Commun.* **2018**, 54, 14097-14099.
12. Wang, L.; Zhang, Y.; Hu, H.; Shi, H.; Song, Y.; Guo, D.; Liu, X.; Sun, X. A $Zn(ClO_4)_2$ Electrolyte Enabling Long-Life Zinc Metal Electrodes for Rechargeable Aqueous Zinc Batteries. *ACS Appl. Mater. Interfaces* **2019**, 11, 42000-42005.

13. Song, M.; Tan, H.; Chao, D.; Fan, H. J. Recent Advances in Zn-Ion Batteries. *Adv. Funct. Mater.* **2018**, 28, 1802564.
14. Wang, F.; Borodin, O.; Gao, T.; Fan, X.; Sun, W.; Han, F.; Faraone, A.; Dura, J. A.; Xu, K.; Wang, C. Highly Reversible Zinc Metal Anode for Aqueous Batteries. *Nat. Mater.* **2018**, 17, 543-549.
15. Zhang, N.; Cheng, F.; Liu, Y.; Zhao, Q.; Lei, K.; Chen, C.; Liu, X.; Chen, J. Cation-Deficient Spinel $ZnMn_2O_4$ Cathode in $Zn(CF_3SO_3)_2$ Electrolyte for Rechargeable Aqueous Zn-Ion Battery. *J. Am. Chem. Soc.* **2016**, 138, 12894-12901.
16. Soundharrajan, V.; Sambandam, B.; Kim, S.; Islam, S.; Jo, J.; Kim, S.; Mathew, V.; Sun, Y. K.; Kim, J. The Dominant Role of Mn^{2+} Additive on the Electrochemical Reaction in $ZnMn_2O_4$ Cathode for Aqueous Zinc-Ion Batteries. *Energy Storage Mater.* **2020**, 28, 407-417.
17. Xu, D.; Li, B.; Wei, C.; He, Y. B.; Du, H.; Chu, X.; Qin, X.; Yang, Q. H.; Kang, F. Preparation and Characterization of MnO_2/Acid-Treated CNT Nanocomposites for Energy Storage with Zinc Ions. *Electrochim. Acta* **2014**, 133, 254-261.
18. Mo, F.; Li, H.; Pei, Z.; Liang, G.; Ma, L.; Yang, Q.; Wang, D.; Huang, Y.; Zhi, C. A Smart Safe Rechargeable Zinc Ion Battery Based on Sol-Gel Transition Electrolytes. *Sci. Bulletin.* **2018**, 63, 1077-1086.
19. Shi, H.; Ye, Y.; Liu, K.; Song, Y.; Sun, X. A Long-Cycle-Life Self-Doped Polyaniline Cathode for Rechargeable Aqueous Zinc Batteries. *Angew. Chem., Int. Ed.* **2018**, 57, 16359-16363.
20. Li, C.; Xie, X.; Liang, S.; Zhou, J. Issues and Future Perspective on Zinc Metal Anode for Rechargeable Aqueous Zinc-Ion Batteries. *Energy Environ. Mater.* **2020**, 3, 146-159.
21. Lu, W.; Xie, C.; Zhang, H.; Li, X. Inhibition of Zinc Dendrite Growth in Zinc-Based Batteries. *ChemSusChem* **2018**, 11, 3996-4006.
22. Xie, C.; Li, Y.; Wang, Q.; Sun, D.; Tang, Y.; Wang, H. Issues and Solutions Toward Zinc Anode in Aqueous Zinc-Ion Batteries: a Mini Review *Carbon Energy* **2020**, 2, 540-560.
23. Dong, L.; Yang, W.; Yang, W.; Tian, H.; Huang, Y.; Wang, X.; Xu, C.; Wang, C.; Kang, F.; Wang, G. Flexible and Conductive Scaffold-Stabilized Zinc Metal Anodes for Ultralong-Life Zinc-Ion Batteries and Zinc-Ion Hybrid Capacitors. *Chem. Eng. J.* **2019**, 384, 123355.
24. Tian, Y.; An, Y.; Wei, C.; Xi, B.; Xiong, S.; Feng, J.; Qian, Y. Flexible and Free-Standing $Ti_3C_2T_x$ MXene@Zn Paper for Dendrite-Free Aqueous Zinc Metal Batteries and Nonaqueous Lithium Metal Batteries. *ACS Nano* **2019**, 13, 11676-11685.
25. Wang, Z.; Huang, J.; Guo, Z.; Dong, X.; Liu, Y.; Wang, Y.; Xia, Y. A Metal-Organic Framework Host for Highly Reversible Dendrite-Free Zinc Metal Anodes. *Joule* **2019**, 3, 1289-1300.

26. Li, C.; Shi, X.; Liang, S.; Ma, X.; Han, M.; Wu, X.; Zhou, J. Spatially Homogeneous Copper Foam as Surface Dendrite-Free Host for Zinc Metal Anode. *Chem. Eng. J.* **2020**, 379, 122248.
27. Zhao, K.; Wang, C.; Yu, Y.; Yan, M.; Wei, Q.; He, P.; Dong, Y.; Zhang, Z.; Wang, X.; Ma, L. Ultrathin Surface Coating Enables Stabilized Zinc Metal Anode. *Adv. Mater. Interfaces* **2018**, 5, 1800848.
28. Liang, P.; Yi, J.; Liu, X.; Wu, K.; Wang, Z.; Cui, J.; Liu, Y.; Wang, Y.; Xia, Y.; Zhang, J. Highly Reversible Zn Anode Enabled by Controllable Formation of Nucleation Sites for Zn-Based Batteries. *Adv. Funct. Mater.* **2020**, 30, 1908528.
29. Zhang, N.; Huang, S.; Yuan, Z.; Zhu, J.; Zhao, Z. Direct Self-Assembly of MXene on Zn Anodes for Dendrite-Free Aqueous Zinc-Ion Batteries. *Angew. Chem., Int. Ed.* **2021**, 133, 2897.
30. Deng, C.; Xie, X.; Han, J.; Tang, Y.; Gao, J.; Liu, C.; Shi, X.; Zhou, J.; Liang, S.; A Dieve-Functional and Uniform-Porous Kaolin Layer Toward Stable Zinc Metal Anode. *Adv. Funct. Mater.* **2020**, 30, 2000599.
31. Liu, M.; Yang, L.; Liu, H.; Amine, A.; Zhao, Q.; Song, Y.; Yang, J.; Wang, K.; Pan, F., Artificial Solid-Electrolyte Interface Facilitating Dendrite-Free Zinc Metal Anodes via Nanowetting Effect. *ACS Appl. Mater. Interfaces* **2019**, 11 (35), 32046-32051.
32. Zhang, Q.; Luan, J.; Fu, L.; Wu, S.; Tang, Y.; Ji, X.; Wang, H. The Three-Dimensional Dendrite-Free Zinc Anode on a Copper Mesh with a Zinc-Oriented Polyacrylamide Electrolyte Additive. *Angew. Chem., Int. Ed.* **2019**, 58, 15841-15847.
33. Xu, W.; Zhao, K.; Huo, W.; Wang, Y.; Yao, G.; Gu, X.; Cheng, H.; Mai, L.; Hu, C.; Wang, X. Diethyl Ether as Self-Healing Electrolyte Additive Enabled Long-Life Rechargeable Aqueous Zinc Ion Batteries. *Nano Energy* **2019**, 62, 275-281.
34. Bayaguud, A.; Luo, X.; Fu, Y.; Zhu, C. Cationic Surfactant-Type Electrolyte Additive Enables Three-Dimensional Dendrite-Free Zinc Anode For Stable Zinc-Ion Batteries. *ACS Energy Lett.* **2020**, 5, 3012-3020.
35. Yang, W.; Du, X.; Zhao, J.; Chen, Z.; Cui, G., Hydrated Eutectic Electrolytes with Ligand-Oriented Solvation Shells for Long-Cycling Zinc-Organic Batteries. *Joule* **2020**, 4.
36. Hao, J.; Long, J.; Li, B.; Li, X.; Zhang, S.; Yang, F.; Zeng, X.; Yang, Z.; Pang, W. K.; Guo, Z. Toward High-Performance Hybrid Zn-Based Batteries via Deeply Understanding Their Mechanism and Using Electrolyte Additive. *Adv. Funct. Mater.* **2019**, 29, 1903605.
37. Gautam, G. S.; Senftle, T. P.; Carter, E. A. Understanding the Effects of Cd and Ag Doping in Cu_2ZnSnS_4 Solar Cells. *Chem. Mater.* **2018**, 30, 4543−4555.
38. Wu, L.; Dey, S.; Gong, M.; Liu, F.; Castro, R. H. R. Surface Segregation on Manganese Doped Ceria Nanoparticles and Relationship with Nanostability. *J. Phys. Chem. C* **2014**, 118, 30187−30196.
39. Kim, H. I.; Shin, H. C. SnO Additive for Dendritic Growth Suppression of Electrolytic Zinc. *J. Alloys Compd.* **2015**, 645, 7–10.

40. Fan, X.; Yang, H.; Wang, X.; Han, J.; Wu, Y.; Gou, L.; Li, D.; Ding, Y. Enabling Stable Zn Anode via a Facile Alloying Strategy and 3D Foam Structure. *Adv. Mater. Interfaces* 2021, 8, 2002184
41. Li, Q.; Wang, Y.; Mo, F.; Wang, D.; Liang, G.; Zhao, Y.; Yang, Q.; Huang, Z.; Zhi, C., Calendar Life of Zn Batteries Based on Zn Anode with Zn Powder/Current Collector Structure. *Adv. Energy Mater.* **2021**, 11, 2003931.
42. Guo, W.; Zhang, Y.; Tong, X.; Wang, X.; Zhang, L.; Xia, X.; Tu, J. Multifunctional Tin Layer Enabled Long-Life and Stable Anode for Aqueous Zinc Ion Batteries. *Mater. Today Energy* **2021**, 38, 100675.
43. Blöchl, E. Projector Augmented-Wave Method. *Phys. Rev. B* **1994**, 50, 17953–17979.
44. Perdew, J. P.; Burke, K.; Ernzerhof, M. Generalized Gradient Approximation Made Simple. *Phys. Rev. Lett.***1996**, 77, 3865.
45. Dudarev, S. L.; Bottn, G. A.; Savrasov, S. Y.; Humphreys, C. J.; Sutton, A. P. Electron-Energy-Loss Spectra and the Structural Stability of Nickel Oxide: An LSDA + U Study. *Phys. Rev. B* **1998**,57,1505.
46. Naveed, A.; Yang, H.; Yang, J.; Nuli, Y.; Wang, J. Highly Reversible and Rechargeable Safe Zn Batteries Based on a Triethyl Phosphate Electrolyte. *Angew. Chem., Int. Ed.* **2019**, 58, 2760-2764.
47. Yang, H.; Chang, Z.; Qiao, Y.; Deng, H.; Mu, X.; He, P.; Zhou, H. Constructing a Super-Saturated Electrolyte Front Surface for Stable Rechargeable Aqueous Zinc Batteries. *Angew. Chem., Int. Ed.* **2020**, 59, 9377-9381.
48. He, P.; Huang, J. Detrimental Effects of Surface Imperfections and Unpolished Edges on the Cycling Stability of a Zinc Foil Anode. *ACS Energy Lett.* **2021**, 1990-1995.
49. Zhang, J.; Zhao, J.; Du, H.; Zhang, Z.; Wang, S.; Cui, G. Amide-Based Molten Electrolyte with Hybrid Active Ions for Rechargeable Zn Batteries. *Electrochim. Acta* **2018**, 280, 108-113.
50. Yin, Y.; Wang, S.; Zhang, Q.; Song, Y.; Chang, N.; Pan, Y.; Zhang, H.; Li, X. Dendrite-Free Zinc Deposition Induced by Tin-Modified Multifunctional 3D Host for Stable Zinc-Based Flow Battery. *Adv. Mater.* **2020**, 32, 1906803.
51. Han, Q.; Chi, X.; Zhang, S.; Liu, Y.; Zhou, B.; Yang, J.; Liu, Y. Durable Flexible Self-Standing Hydrogel Electrolytes Enabling High-Safety Rechargeable Solid-State Zinc Metal Batteries. *J. Mater. Chem. A* **2018**, 6, 23046-23054.
52. Tang, Y.; Liu, C.; Zhu, H.; Xie, X.; Gao, J.; Deng, C.; Han, M.; Liang, S.; Zhou, J. Ion-Confinement Effect Enabled by Gel Electrolyte for Highly Reversible Dendrite-Free Zinc Metal Anode. *Energy Storage Mater.* **2020**, 27, 109-116.
53. Zhao, J.; Zhang, J.; Yang, W.; Chen, B.; Zhao, Z.; Qiu, H.; Dong, S.; Zhou, X.; Cui, G.; Chen, L. "Water-in-Deep Eutectic Solvent" Electrolytes Enable Zinc Metal Anodes for Rechargeable Aqueous Batteries. *Nano Energy* **2019,** 57, 625-634.

54. Wang, Z.; Hu, J.; Han, L.; Wang, Z.; Wang, H.; Zhao, Q.; Liu, J.; Pan, F. A MOF-Based Single-Ion Zn^{2+} Solid Electrolyte Leading to Dendrite-Free Rechargeable Zn Batteries. *Nano Energy* **2019,** 56, 92-99
55. Myers, H. P.; Meyers, H. P. *Introductory Solid State Physics*, CRC Press, Boca Raton, FL, USA, **1997**.
56. Jain, V. K.; Kumar, P.; Kumar, M.; Jain, P. ; Bhandari, D.; Vijay, Y. K. Study of Post Annealing Influence on Structural, Chemical and Electrical Properties of ZTO Thin Films. *J. Alloys Compd.* **2011**, 509, 3541-3546.
57. Lee, S.; Park, J.; Oh, J.; Kang, Y. Effect of Compositional Ratio of Sn in SnZn Thin Films on Morphological and Chemical Properties. *Physica B* **2020**, 591, 412257.
58. Zhang, Y.; Shao, Y.; Liu, X.; Shi, C.; Wang, Y.; Meng, G.; Zeng, X.; Yang, Y. A Study on Corrosion Protection of Different Polyaniline Coatings for Mild Steel. *Prog. Org. Coat.* **2017**, 111, 240-247.
59. Kim, H. S.; Jo, Y. N.; Lee, W. J.; Kim, K. J.; Lee, C. W. Coating on Zinc Surface to Improve the Electrochemical Behavior of Zinc Anodes for Zinc-Air Fuel Cells. *Electroanalysis* **2015**, 27, 517-523.
60. Sun, T.; Li, Z.; Zhi, Y.; Huang, Y.; Fan, H. J.; Zhang, Q. Poly(2,5-Dihydroxy-1,4-Benzoquinonyl Sulfide) as an Efficient Cathode for High-Performance Aqueous Zinc–Organic Batteries. *Adv. Funct. Mater.* **2021**
61. Xie, J.; Zhang, Q. Recent Progress in Multivalent Metal (Mg, Zn, Ca, and Al) and Metal-Ion Rechargeable Batteries with Organic Materials as Promising Electrodes. *Small* 2019.
62. Xie, J.; Yu, F.; Zhao, J.; Guo, W.; Zhang, H. L.; Cui, G.; Zhang, Q. An Irreversible Electrolyte Anion-doping Strategy Toward a Superior Aqueous Zn-Organic Battery. *Energy Storage Mater*. **2020**, 33, 283-289.

Tabel of Contents

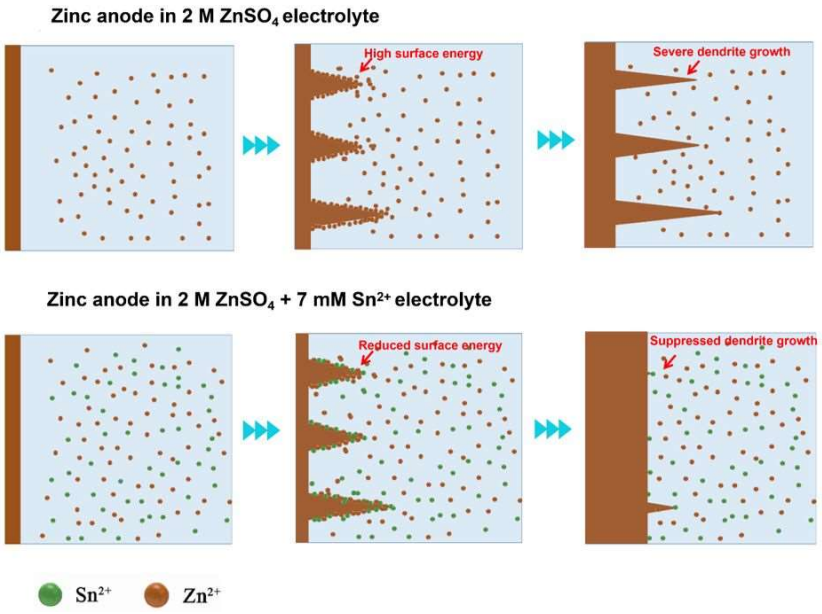

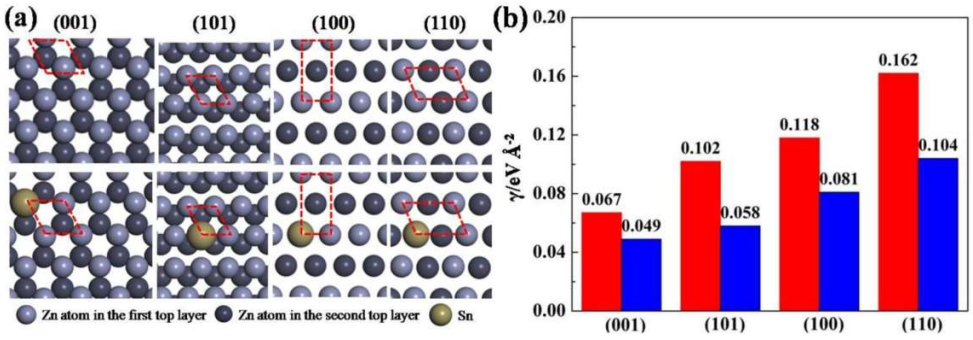

Figure 1. (a) The atomic configuration of the top and second layer of (001), (101), (100) and (110) surfaces of bare and Sn-doped Zn. (b) The comparison of surface free energy without (in red) and with (in blue) Sn dopant.

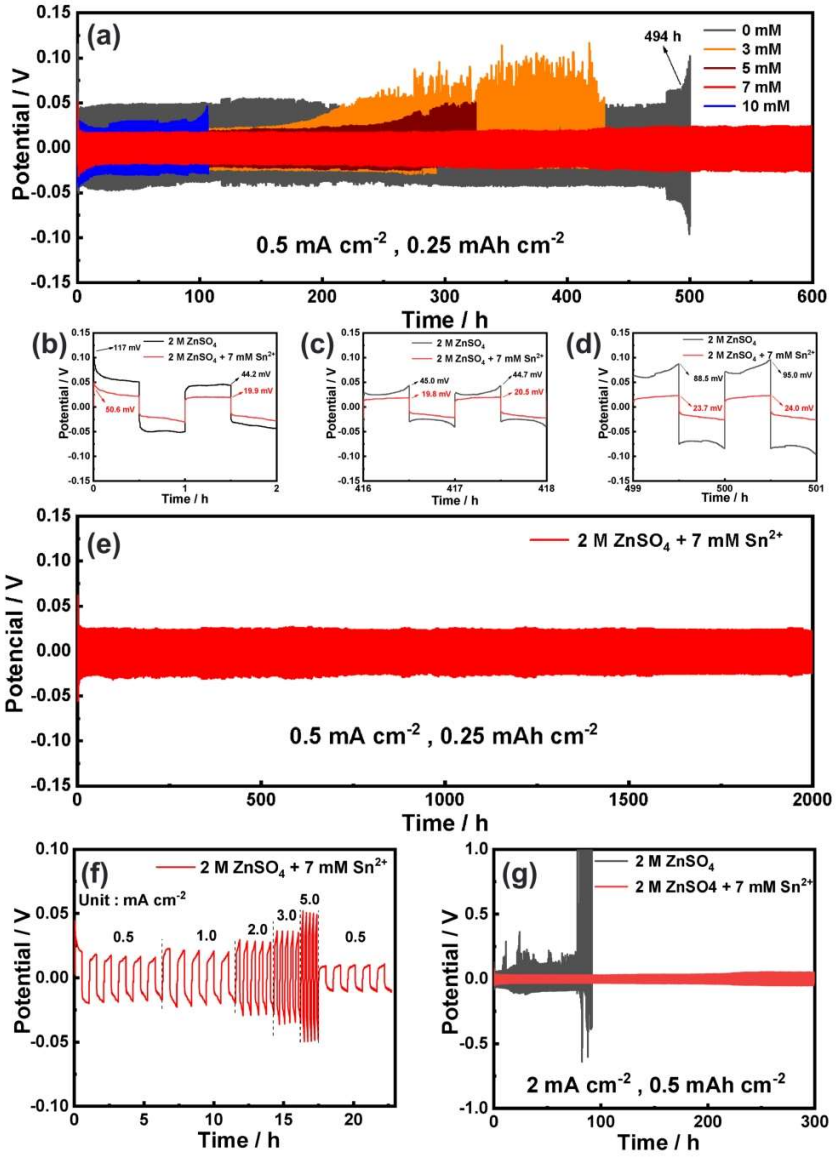

Figure 2. (a) Polarization curves of Zn‖Zn symmetric cells without and with SnCl2 additive in different concentrations at a constant current density of 0.5 mA cm−2, and (b-d) corresponding amplification of the polarization curves in different intervals. (e,f) Long-lifespan polarization curves and rate performance of Zn‖Zn symmetric cells using 2.0 M ZnSO4 +7.0 mM SnCl2 solution as electrolyte. (g) Polarization curves of Zn‖Zn symmetric cells without and with 7.0 mM SnCl2 additive at a high current density of 2 mA cm−2.

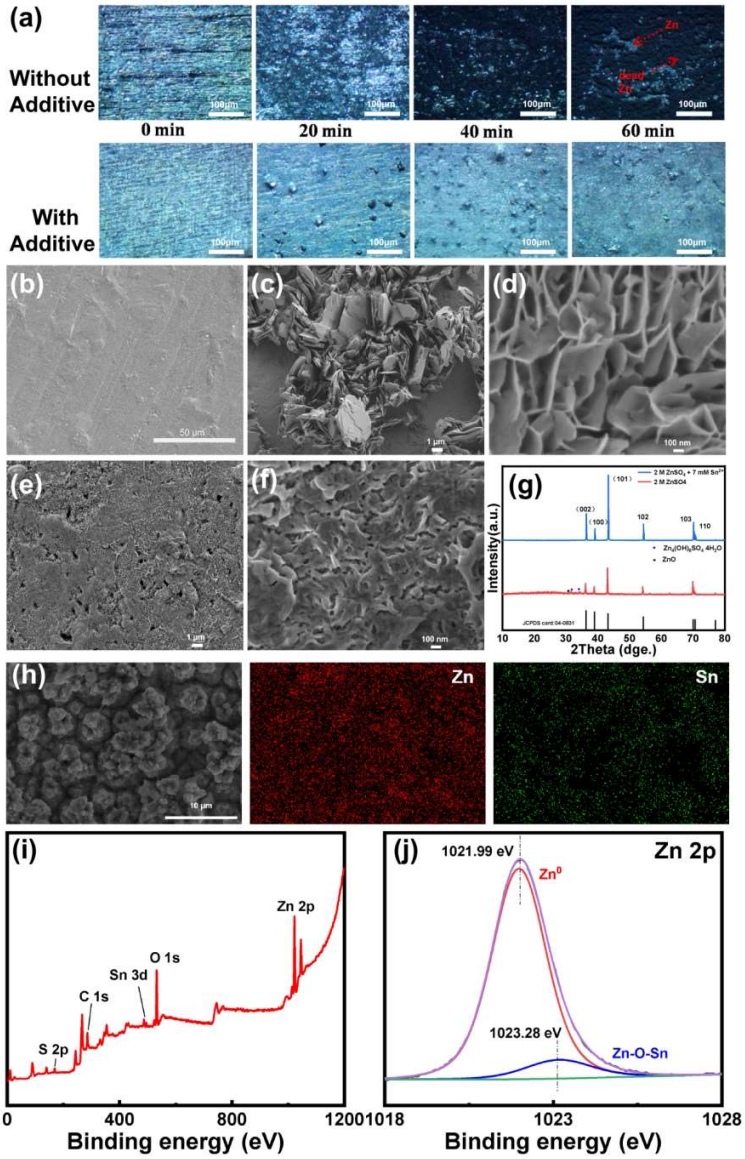

Figure 3. (a) Ex-situ optical microcopy images of the Zn deposition process at a current density of 10 mA cm−2 in 2.0 M ZnSO4 electrolyte without and with 7.0 mM SnCl2 additive. SEM images of (b) bare Zn foil, (c,d) Zn anode in 2.0 M ZnSO4 electrolyte without SnCl2 additive and (e,f) with 7.0 mM SnCl2 additive after 500 cycles at current density of 0.5 mA cm−2. (g) XRD patterns of Zn electrode after 100 cycles at current density of 0.5 mA cm−2 in 2.0 M ZnSO4 electrolyte without and with 7.0 mM SnCl2 additive. (h) EDS-Mapping spectra of copper electrode surface after 10 cycles of Zn/Cu asymmetric battery in electrolyte containing SnCl2. (i) The high resolution XPS spectrum and (j) the deconvoluted spectrum for Zn 2p of Zn anode in Zn‖Zn symmetric cell with SnCl2 additive after 500 plating/stripping cycling.

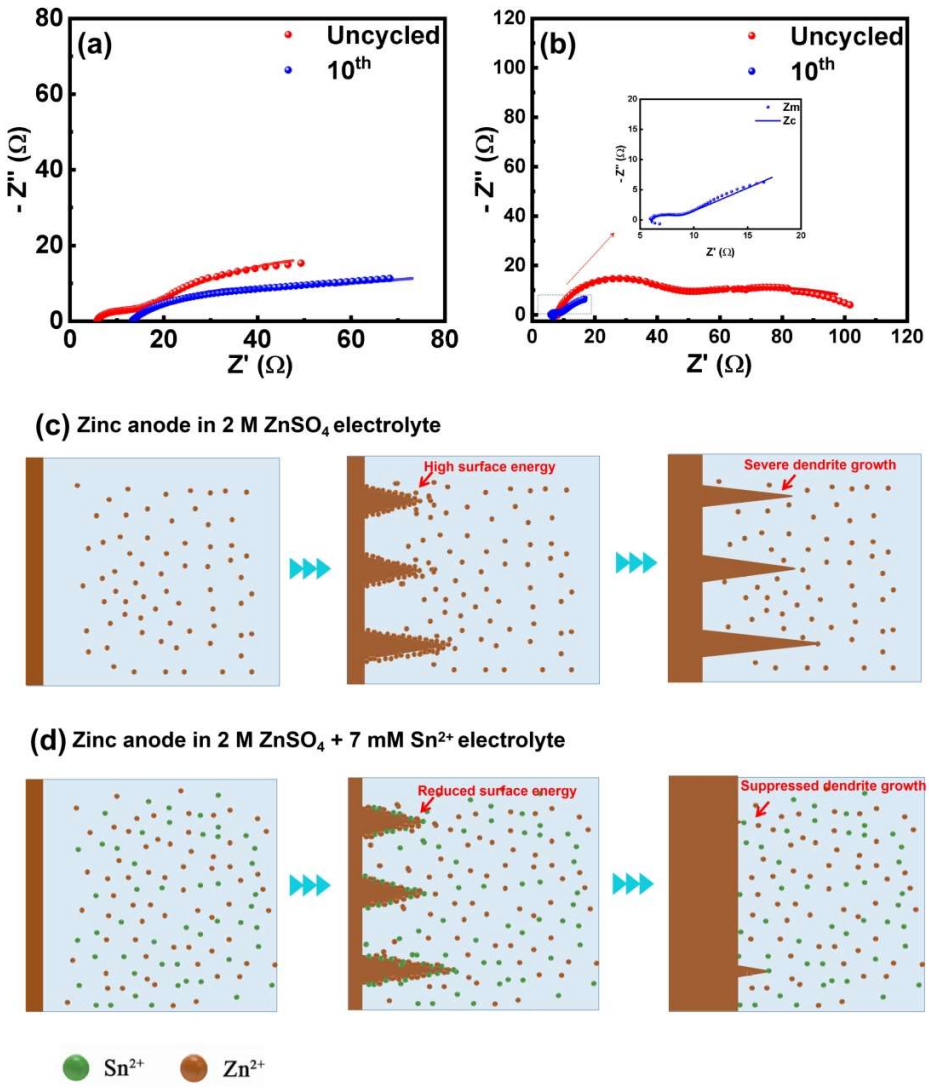

Figure 4. The electrochemical impedance spectra of Zn electrode using ZnSO4 electrolyte (a) without additive and (b) with SnCl2 additive before cycling and after 10 cycles. A three-electrode system with Zn plate as working electrode, Pt plate as counter electrode and Ag/AgCl as reference electrode was constructed. (c-d) The schematic diagram of the interfacial reaction on Zn anode in 2.0 M ZnSO4 electrolyte without/with 7.0 mM SnCl2 additive.

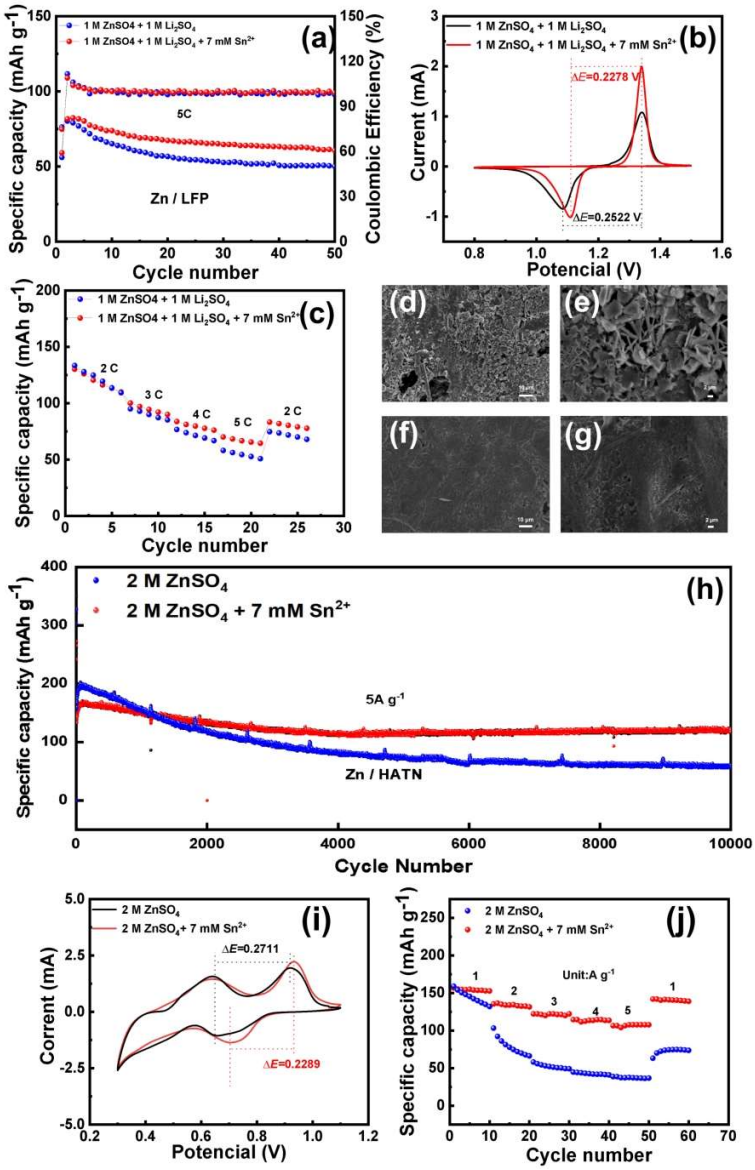

Figure 5. (a) High-rate cycling performances at current density of 5 C (1C = 170 mAh g-1) and (b) CV curves at scan rate of 0.1 mV s−1 between 0.8 and 1.5 V of Zn/LFP full cells without/with additive. (c) Rate capabilities of Zn-LFP batteries at various current rates. SEM images of Zn anode in Zn/LFP coin cells after 50 cycles (d,e) without additive and (f,g) with 7.0 Mm SnCl2 additive. (h) Long-lifespan cycling performance of Zn/HATN full cells under a current density of 5 A g-1. (i) The CV curves of aqueous Zn/HATN batteries (5 mV s-1). (j) Rate capabilities of Zn/HATN batteries at various current rates.